Influence of FCGR3A-158V/F Genotype and Baseline CD20 Antigen Count on Target-Mediated Elimination of Rituximab in Patients with Chronic Lymphocytic Leukemia: A Study of FILO Group

Mira Tout, Anne-Laure Gagez, Stéphane Lepretre, Valérie Gouilleux-Gruart, Nicolas Azzopardi, Alain Delmer, Mélanie Mercier, Loic Ysebaert, Kamel Laribi, Hugo Gonzalez, et al.

Influence of *FCGR3A*-158V/F Genotype and Baseline CD20 Antigen Count on Target-Mediated Elimination of Rituximab in Patients with Chronic Lymphocytic Leukemia: A Study of FILO Group

Mira Tout[1], Anne-Laure Gagez[2,3], Stéphane Leprêtre[4], Valérie Gouilleux-Gruart[5], Nicolas Azzopardi[1], Alain Delmer[6], Mélanie Mercier[7], Loïc Ysebaert8, Kamel Laribi[9], Hugo Gonzalez[10], Gilles Paintaud[1,11], Guillaume Cartron[2,3], David Ternant[1,11]

Abstract

Background and objectives Rituximab is an anti-CD20 monoclonal antibody approved in the first-line treatment of patients with chronic lymphocytic leukemia (CLL). Rituximab pharmacokinetics shows a time dependency possibly related to changes in the target antigen amount over time. The purpose of this study was to quantify the influence of both CD20 antigenic mass and the FcγRIIIA genetic polymorphism on rituximab pharmacokinetics in CLL.

Methods Rituximab pharmacokinetics was described in 118 CLL patients using a semi-mechanistic model including a latent target antigen turnover, which allowed the estimation of rituximab target-mediated elimination in addition to the endogenous clearance.

Results Target-mediated elimination rate constant increased with the baseline CD20 count on circulating B cells ($p = 0.00046$) and in patients with the *FCGR3A*-158VV genotype ($p = 0.0016$). Physiologic elimination of antigen was lower in the Binet C disease stage ($p = 0.00018$). The effects of these covariates on rituximab concentrations were mainly visible at the beginning of treatment. Body surface area also increased central and peripheral volumes of distribution ($p = 1.3 \times 10^{-5}$ and 0.0015, respectively).

Conclusions A pharmacokinetic model including target-mediated elimination accurately described rituximab concentrations in CLL and showed that rituximab 'consumption' (target-mediated elimination) increases with increasing baseline antigen count on circulating B cells and in *FCGR3A*-158VV patients.

Clinical trial registration: NCT01370772.

✉ David Ternant
david.ternant@univ-tours.fr

[1] Université François-Rabelais de Tours, CNRS, GICC UMR 7292, Tours, France

[2] Université de Montpellier, CNRS, UMR 5235, Montpellier, France

[3] Department of Hematology, CHU Montpellier, Montpellier, France

[4] Department of Hematology, Henri Becquerel Center, Rouen, France

[5] Laboratory of Immunology, CHU de Tours, Tours, France

[6] Department of Hematology, CHU de Reims, Reims, France

[7] Department of Hematology, CHU Angers, Angers, France

[8] Department of Hematology, CHU Toulouse, Toulouse, France

[9] Department of Hematology, CHG Le Mans, Le Mans, France

[10] Department of Hematology, CHG Pontoise, Pontoise, France

[11] Laboratory of Pharmacology-Toxicology, CNRS, UMR 7292, CHU de Tours, 2 boulevard Tonnellé, 37044 Tours Cedex, France

Key Points

Rituximab, an anti-CD20 monoclonal antibody, was previously shown to exhibit time-dependent clearance in chronic lymphocytic leukemia, suggesting an impact of variations in antigenic mass on clearance.

For the first time in chronic lymphocytic leukemia patients, rituximab pharmacokinetics was described using a semi-mechanistic model including the target-mediated elimination of rituximab. An increase in target-mediated elimination, hence in rituximab 'consumption' (target-mediated elimination) was shown with a higher baseline CD20 amount and for the *FCGR3A*-158VV genotype, which was associated with lower rituximab concentrations in early treatment cycles.

1 Introduction

Rituximab is a chimeric IgG1 monoclonal antibody targeting the CD20 antigen expressed on the surface of most normal and malignant B cells. It has improved clinical outcomes in chronic lymphocytic leukemia (CLL) [1–3] and has become the standard-of-care treatment for this disease.

Some studies reported a large interindividual variability in rituximab pharmacokinetics (PK) [4, 5]. This variability is relevant because higher rituximab exposure is associated with better clinical outcomes in CLL [5], as well as in other B-cell malignancies [4, 6, 7]. Previous studies suggested that rituximab PK may be influenced by the antigenic burden; in patients with recurrent low-grade lymphoma, lower tumor volume and lymphocyte count at baseline were associated with higher rituximab serum concentrations [4]. In a murine model of lymphoma expressing human CD20, an increase in tumor volume was associated with increased rituximab clearance [8]. This may be explained by target-mediated drug disposition (TMDD), referring to rituximab PK that is influenced by its interaction with the target antigen. TMDD models were shown to be suitable to account for the nonlinear nature of the PK of several monoclonal antibodies [9–12]. In CLL patients, rituximab was shown to exhibit a time-dependent elimination, with a clearance monoexponentially decreasing over time [5]. Although this decrease in clearance could possibly reflect the treatment-related decrease in antigenic burden over time, the influence of antigenic burden on rituximab elimination has never been assessed.

Several other factors may explain rituximab pharmacokinetic variability, including the single nucleotide polymorphism of *FCGR3A*, which encodes FcγRIIIa with either a valine (V) or a phenylalanine (F) at position 158. FcγRIIIa is a receptor binding the Fc portion of IgG, expressed on macrophages and natural killer cells, the main actors of antibody-dependent cellular cytotoxicity (ADCC), which is a key mechanism by which rituximab induces target-cell lysis [13]. In vitro, a higher affinity of human IgG1 towards FcγRIIIa-158V compared with FcγRIIIa-158F has been shown [14]. In vivo, in B-cell malignancies, the influence of the *FCGR3A*-158V/F polymorphism was reported in patients with follicular lymphoma [15, 16] and diffuse large B-cell lymphoma [17] with higher response rates for homozygous *FCGR3A*-158V patients, but not in CLL [18, 19]. This polymorphism was shown to influence the PK of infliximab, an anti-tumor necrosis factor-α monoclonal antibody [20]. This could possibly be explained by increased target-mediated elimination in *FCGR3A*-158VV patients, a hypothesis that has not been confirmed mechanistically. The possible influence of the *FCGR3A*-158V/F polymorphism on rituximab PK has never been investigated.

The present study aimed at investigating the influence of both baseline antigen burden and the *FCGR3A*-158V/F polymorphism on rituximab PK in CLL patients.

2 Patients and Methods

2.1 Study

This ancillary pharmacokinetic study was part of a prospective phase II, multicenter, randomized trial, CLL 2010 FMP (NCT01370772), designed to explore intensified rituximab pre-phase monotherapy before a standard fludarabine-cyclophosphamide-rituximab (R-FC) regimen in previously untreated, symptomatic B-cell CLL patients. The study was approved by the Ethics Committee of the French South Region II. All patients signed written informed consent before inclusion. Briefly, eligible patients were those aged between 18 and 66 years, with immunophenotypically confirmed untreated CLL according to International Workshop on Chronic Lymphocytic Leukemia 2008 criteria [21], Matutes score of 4 or 5, and Binet stage C or A and B with active disease [21, 22]. Patients were excluded if they had 17p deletion (fluorescence in situ hybridization >10% positive nuclei), human immunodeficiency virus seropositivity, or known hypersensitivity to humanized monoclonal antibodies or any of the study drugs. Patients were randomly assigned to two treatment groups: the first group (standard R-FC arm)

received R-FC every 28 days for six treatment cycles, where rituximab (MabThera®; Roche, Basel, Switzerland) was administered intravenously at a dose of 375 mg/m^2 in cycle 1, followed by 500 mg/m^2 in cycles 2–6. In the experimental group (dense R-FC arm), patients received a pre-phase of intravenous rituximab at doses of 500 mg on day 0, and 2000 mg on days 1, 8, and 15, followed by six cycles of 500 mg/m^2 intravenous rituximab in combination with FC, starting on day 22 and repeated every 28 days.

2.2 Data

In both arms, rituximab serum concentrations were measured before and after each rituximab infusion. Additional samples were obtained 3 and 6 months after the end of treatment. Rituximab concentrations were measured using an enzyme-linked immunosorbent assay derived from a previously validated technique [23]. The limit of detection was 0.061 mg/L and the lower and upper limits of quantification were 0.20 and 9.0 mg/L, respectively. The inter-day accuracy was 14–16%, and the precision ranged from 5 to 13%.

FCGR3A genotyping was performed using a technique derived from Dall'Ozzo et al. [24]. Patients were staged using the Binet system into categories of low (stage A, three or fewer areas of lymphoid involvement), intermediate (stage B, three or more areas of lymphoid involvement), or high risk (stage C, anemia and/or thrombocytopenia) [22, 25].

A whole-body computed tomography scan (neck, thorax, abdomen, and pelvis) was conducted on the pre-inclusion visit and on M9 (9 months after the first treatment day, and at least 3 months after the end of treatment). Three-dimensional tumor volume measurements of the six largest lesions were performed according to an accurate semi-automated measurement technique with thin slicing [26].

CD20 expression at baseline was quantified using the QuantiBRITE® flow cytometry system (BD Biosciences, Le Pont-de-Claix, France). Using a calibration curve, CD20 fluorescence intensity determined using 8-peak Rainbow bead calibration particles (Spherotech, Lake Forest, IL, USA) was converted to molecules of equivalent soluble fluorochrome, which represents the number of CD20 molecules per cell.

Baseline total count of the CD20 antigenic target was quantified on B cells both in the circulation ($CD20_{cir}$) and in the lymph nodes ($CD20_{LN}$), as follows:

$$CD20_{cir} = \text{CD20 expression per cell} \times \text{number of circulating target cells},$$

$$CD20_{LN} = \text{CD20 expression per cell} \times \text{number of cells for six scanned lesions},$$

where CD20 expression per cell is expressed in molecules of equivalent soluble fluorochrome, number of circulating target cells is $CD19^+$ cell concentration × blood volume, $CD19^+$ cell concentration is total lymphocyte concentration × % $CD19^+$ cells, and blood volume is calculated according to Pearson et al. [27]. The number of cells for six scanned lesions is the volume of six scanned lesions (cm^3)/CLL lymphocyte volume, where the CLL lymphocyte volume is assumed to be 54×10^{-12} cm^3 [28].

2.3 Pharmacokinetic Analysis

Pharmacokinetic data were analyzed with a population approach using the non-linear mixed-effects modeling software Monolix® version 4.3.3 (Lixoft®, Orsay, France). The Monte Carlo importance sampling and stochastic approximation expectation-maximization methods were used for likelihood estimation. To ensure the best possible convergence of the stochastic approximation expectation-maximization algorithm, 1000 K1 and 300 K2 iteration kernels were used.

As usually reported for the PK of monoclonal antibodies, we tested a two-compartment model, with (1) a linear elimination, (2) a parallel linear and target-mediated Michaelis–Menten elimination, or (3) a clearance composed of a time-independent term, and a time-dependent term exponentially decreasing with time. (4) Additionally, a semi-mechanistic model including a latent target antigen turnover was tested. This latter model was developed on the basis of a transit model of Friberg et al. [29] applied previously to describe cell maturation processes in chemotherapy-induced neutropenia [29] and thrombocytopenia [30]. The latent transit model describes CD20-expressing B-cell maturation from progenitor to mature cells through transit compartments. These compartments were latent because the CD20 amount was not measured over time. The latent variable represents the latent amount of CD20 expressed on mature B cells available for rituximab binding. Target antigen is produced in the first compartment at a zero-order rate constant k_{in}. The transfer rate between transit compartments is described by a first-order rate constant k_{tr}. The time between the progenitor stage to cell maturation is defined as the mean transit time MTT, calculated as $(n + 1)/k_{tr}$, where n is the number of transit compartments. Endogenous elimination of target is described by the first-order rate constant k_{out}. Rituximab elimination consists in both (1) linear (endogenous) clearance CL and (2) second-order target-mediated elimination rate constant k_{deg}. Different numbers of transit compartments were evaluated, as well as target-mediated elimination from different target-antigen compartments. Estimated parameters in the final model were CL, distribution clearance (Q), central (V_1), and peripheral (V_2) volumes of distribution, MTT, k_{in}, k_{out}, and k_{deg}. Furthermore, we tested the inclusion of a feedback loop accounting for

cytokine response to variations in cell count, associated with a first-order constant k_{in}, as previously described for neutrophil maturation and chemotherapy-induced myelosuppression [29].

Interindividual variability of the model parameters was described using an exponential error model, defined as $\theta_i = \theta_{TV} \times e^{i}$, where θ_i is the parameter value in the ith subject, θ_{TV} is the typical value of the parameter in the population, and i is the individual deviation from the typical value, with mean zero and variance ω^2. The residual variability was modeled with a mixed additive-proportional error model: $C_{ij,obs} = C_{ij,pred} \times (1 + \varepsilon_{ij,prop}) + \varepsilon_{ij,add}$, where $C_{ij,obs}$ and $C_{ij,pred}$ are the jth observed and predicted concentrations, respectively, for the ith subject, and $\varepsilon_{ij,prop}$ and $\varepsilon_{ij,add}$ are the proportional and additive residual errors, respectively, with means zero and respective variances of ${\sigma_{prop}}^2$ and ${\sigma_{add}}^2$.

2.4 Covariate Analysis

Evaluated covariates were demographic factors (sex, age, body size), treatment arm, variables reflecting antigenic burden/disease severity ($CD20_{cir}$, $CD20_{LN}$, Binet stage), *FCGR3A*-158V/F genetic polymorphism, and albuminemia. The influence of a binary covariate (CAT) on a parameter was implemented as: $\ln(\theta_{TV}) = \ln(\theta_{CAT=0}) + \beta_{CAT=1}$, where $\theta_{CAT=0}$ is the value of θ for the reference category, and $\beta_{CAT=1}$ is a parameter modifying the typical value for the other category. Continuous covariates were modeled using a power model centered on their median. Covariate selection was based on the likelihood ratio test, where the difference in objective function value (OFV, $-2 \times$ log likelihood) between two nested models is assumed to follow a Chi-square distribution with one degree of freedom. The effect of potential variables on model parameters was tested using a forward-backward stepwise selection process. In the univariate step, covariates showing a significant association with pharmacokinetic parameters ($p < 0.05$, ΔOFV >3.84) were included in the model. In the multivariate step, significant covariates for $p < 0.05$ were included during forward addition, and those significant for $p < 0.01$ were retained during the backward elimination.

2.5 Model Evaluation

Comparison between models was made using OFV in the case of nested models, and Akaike's information criterion (AIC) for non-nested models, where AIC = OFV + $2 \times p$, p being the number of estimated model parameters. All models were evaluated graphically using goodness-of-fit diagnostic plots: observed vs. population and individual predicted concentrations; population and individual weighted residuals vs. time and population predicted concentration. Visual predictive checks and normalized prediction distribution errors [31] were also performed by simulating 1000 replicates using the population model parameters.

2.6 Model-Based Simulations

The final model estimates of the typical parameters (pharmacokineticand covariate parameters) were used to simulate rituximab concentration-time profiles in (1) the standard arm following doses of 375 mg/m^2 in cycle 1 followed by 500 mg/m^2 in cycles 2–6, and in (2) the dense arm following doses of 500 mg on day 0, 2000 mg on days 1, 8, and 15, and 500 mg/m^2 in cycles 1–6. Rituximab concentrations predicted in patients with the given $CD20_{cir}$, *FCGR3A*-158V/F genotype, and Binet stage were compared. Additionally, the data set was simulated 500 times using typical and interindividual parameters of the final model. This allowed estimating 90% prediction intervals of rituximab concentrations and latent amount of CD20 expressed on mature B cells available for rituximab binding (L) for both treatment arms according to *FCGR3A*-158V/F genotype and Binet stage.

3 Results

3.1 Patients

A total of 118 patients were included in this pharmacokinetic study. Of these, 55 patients were in the standard R-FC arm, and 63 patients in the dense R-FC arm. The median [range] age was 58 years [39–65 years], and the majority of patients were male (75%), in Binet stage B with active disease (71%) or C (27%). Median [interquartile range] $CD20_{cir}$ and $CD20_{LN}$ counts were 29×10^{14} [$11–56 \times 10^{14}$] and 102×10^{14} [$53–167 \times 10^{14}$], respectively (Table 1). There were no significant differences in the patient characteristics between the two treatment groups.

3.2 Pharmacokinetic Analysis

A total of 1943 rituximab serum concentrations were available for population analysis, six (0.3%) being below the quantification limit. (1) The two-compartment model with linear elimination (AIC = 21,857) overestimated rituximab trough concentrations during the first cycles, particularly in the standard R-FC arm. (2) Michaelis–Menten elimination terms were not correctly estimated and did not improve model performance (AIC = 22598). (3) Introducing a time-dependent clearance allowed a better estimation of early trough concentrations (AIC = 21,009).

Table 1 Baseline characteristics of the study population

Characteristic	All patients	Standard R-FC arm	Dense R-FC arm	*p* value
Number	118	55	63	
Sex (men/women)	88 (75)/30 (25)	43 (78)/12 (22)	45 (71)/18 (29)	0.52
Age (years)	58 [52–62]	60 [52–62]	58 [53–61]	0.36
Body surface area (m^2)	1.90 [1.76–2.00]	1.93 [1.76–2.00]	1.90 [1.76–1.98]	0.13
Binet stage[a]				0.44
A with active disease	2 (2)	0 (0)	2 (3)	
B with active disease	84 (71)	38 (69)	46 (73)	
C	32 (27)	17 (31)	15 (24)	
Time since diagnosis (months)	28.3 [5.3–48.7]	18.6 [5.5–44.8]	30.8 [5.3–50.82]	0.77
WBC ($\times 10^9$/L)	75 [33–128]	49 [26–106]	94 [43–145]	0.05
Lymphocytes ($\times 10^9$/L)	63 [27–113]	46 [22–98]	89 [41–127]	0.05
$CD19^+$ cells (%)	93 [85–97]	93 [85–97]	93 [83.5–97.5]	0.60
Platelets ($\times 10^9$/L)	155 [121–202]	155 [110–189]	166 [126–210]	0.28
Proteins (g/L)	67 [65–71]	68 [65–71]	67 [64–71]	0.24
Albumin (g/L)	44 [41–47]	45 [43–47]	44 [41–46]	0.06
IgG (g/L)	6.60 [5.15–7.67]	6.60 [5.65–7.42]	6.60 [4.91–8.00]	0.79
CD20 density per cell (MESF)	10,580 [7095–13,980]	10,580 [8864–13,410]	10,580 [6998–14,890]	0.96
$CD20_{cir}$ ($\times 10^{14}$)	29 [11–56]	25 [8–46]	32 [16–59]	0.19
$CD20_{LN}$ ($\times 10^{14}$)	102 [53–167]	103 [58–163]	99 [47–170]	0.90
FCGR3A				0.90
VV	13 (11)	6 (11)	7 (11)	
VF	61 (52)	27 (49)	34 (54)	
FF	44 (37)	22 (40)	22 (35)	

Results are expressed as median [interquartile range] for continuous variables or number (%) for categorical variables. *p* values were obtained with the Mann–Whitney test (continuous variables) or Fisher's exact test (categorical variables)

$CD20_{cir}$ baseline CD20 count on circulating B cells, *$CD20_{LN}$* baseline CD20 count in the lymph nodes, *MESF* molecules of equivalent soluble fluorochrome, *R-FC* fludarabine-cyclophosphamide-rituximab, *WBC* white blood cell count

[a] Binet staging system: stage A, three or fewer areas of lymphoid involvement; stage B, three or more areas of lymphoid involvement; stage C, anemia and/or thrombocytopenia

(4) However, the semi-mechanistic model with a zero-order production constant k_{in} and 3 transit compartments (Fig. 1) allowed the best data description, with an AIC reduction of 555 compared with the latter model (AIC = 20,454). No improvement in pharmacokinetic description was achieved neither by allowing target-mediated elimination from several compartments (ΔAIC = 398) nor by using a first-order progenitor proliferation with feedback from the latent mature B-cell compartment. Notably, the feedback parameter could not be accurately estimated and led to an increase of 860 in AIC.

The inter-individual variability of Q, MTT, and k_{in} was not identifiable and was therefore not estimated and fixed to zero. A large inter-individual variability of 90.5% was observed for k_{deg} compared with a moderate inter-individual variability of 30% for non-specific clearance. All parameters were accurately estimated with relative standard errors $\leq$30% (Table 2). Plots of predicted vs. observed concentrations showed a good agreement of the model, even if a slight overestimation of the lowest concentrations was observed (Fig. 2). Diagnostic plots (population-weighted residuals, individual-weighted residuals, normalized prediction distribution errors, and visual predictive checks) showed no obvious bias or model misspecification (Fig. 2).

In the univariate analysis, CL was found to be influenced by body surface area (BSA), albuminemia, and treatment arm; V_1 was influenced by sex, BSA, and $CD20_{cir}$; V_2 was influenced by sex and BSA; k_{out} was influenced by BSA, $CD20_{cir}$, $CD20_{LN}$, and Binet stage; and k_{deg} was influenced by $CD20_{cir}$, *FCGR3A*-158V/F polymorphism, and treatment arm. In the final model, 32% of the inter-individual variability of k_{deg} was explained by both $CD20_{cir}$ ($p = 0.00046$) and the *FCGR3A*-158V/F polymorphism ($p = 0.0016$). The highest $CD20_{cir}$ of the patient population (402.4×10^{14}) corresponded to a 13-fold higher k_{deg} compared with that associated with the lowest $CD20_{cir}$ (0.12×10^{14}; Fig. 3a).

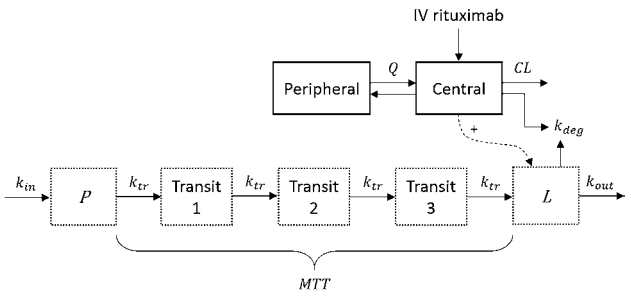

$$\frac{dA_1}{dt} = -(CL + Q) \times \frac{A_1}{V_1} + Q \times \frac{A_2}{V_2} - k_{deg} \times A_1 \times L$$
$$\frac{dA_2}{dt} = Q \times \left(\frac{A_1}{V_1} - \frac{A_2}{V_2}\right)$$
$$\frac{dP}{dt} = k_{in} - k_{tr} \times P, \qquad P(0) = L_{ini}$$
$$\frac{dTransit1}{dt} = k_{tr} \times P - k_{tr} \times Transit1$$
$$\frac{dTransit2}{dt} = k_{tr} \times Transit1 - k_{tr} \times Transit2$$
$$\frac{dTransit3}{dt} = k_{tr} \times Transit2 - k_{tr} \times Transit3, \qquad Transit1,2,3(0) = L_{ini}$$
$$\frac{dL}{dt} = k_{tr} \times Transit3 - k_{out} \times L - k_{deg} \times A_1 \times L, \qquad L(0) = L_{ini}$$
$$k_{tr} = \frac{n+1}{MTT}, \qquad L_{ini} = \frac{k_{in}}{k_{out}}$$

Fig. 1 Schematic of the semi-mechanistic model linking a two-compartment pharmacokinetic model to CD20 target-antigen latent turnover (*dashed compartments*). The latent transit model describes CD20-expressing B-cell maturation from progenitor to mature cells through transit compartments. These compartments were latent because the CD20 amount was not measured over time. Rituximab is eliminated by (1) the endogenous pathway (CL) and (2) the target-mediated pathway (k_{deg}, second-order rate constant). A_1 and A_2 amounts of rituximab in central and peripheral compartments respectively, *IV* intravenous, k_{in} zero-order production rate, k_{out} first-order rate constant of rituximab-independent death of latent target antigen, k_{tr} rate of transit between compartments, L latent amount of CD20 expressed on mature B-cells available for rituximab binding, P latent progenitor compartment, *Transit* latent maturation compartment, Q distribution clearance

Patients with the *FCGR3A*-158VV genotype had a four-fold higher k_{deg} than F carriers (VF and FF; 0.0075 vs. 0.0017 $\text{nmol}^{-1}\ \text{d}^{-1}$; Fig. 3b). A lower k_{out} value was observed in Binet stage C compared with active A and B (11.9×10^{-5} vs. $17.6 \times 10^{-5}\ \text{d}^{-1}$; $p = 0.00018$; Fig. 3c). V_1 and V_2 significantly increased with BSA ($p = 1.3 \times 10^{-5}$ and 0.0015, respectively). Patients in the dense R-FC arm had higher CL ($p = 0.001$) and V_2 ($p = 1.7 \times 10^{-9}$) than those in the standard R-FC arm.

3.3 Model-Based Simulations

The influence of covariates on simulated concentration-time profiles was most obvious in the standard R-FC arm (Fig. 4). Trough concentrations before the second injection were 74% lower for the highest CD20_{cir} than for the lowest CD20_{cir} (Fig. 4a), and 58% lower in *FCGR3A*-158VV patients compared with F carriers (Fig. 4c). These differences became minor after the second treatment cycle.

Table 2 Pharmacokinetic parameter estimates

Parameter (unit)	Estimate	RSE (%)	p value
Fixed effects			
CL (L/d)	0.137	4	
Dense R-FC arm on CL	0.197	29	0.0010
V_1 (L)	3.08	2	
BSA on V_1	0.904	21	1.3×10^{-5}
Q (L/d)	0.31	3	
V_2 (L)	2.54	6	
Dense R-FC arm on V_2	0.52	16	1.7×10^{-9}
BSA on V_2	1.31	30	0.0015
MTT (d)	57.6	5	
k_{in} (nmol/d)	0.22	6	
k_{out} (d^{-1})	17.6×10^{-5}	8	
Binet stage C on k_{out}	−0.392	27	0.00018
k_{deg} ($\text{nmol}^{-1}\text{d}^{-1}$)	0.0017	12	
FCGR3A-158VV on k_{deg}	1.47	25	0.0016
CD20_{cir} on k_{deg}	0.32	25	0.00046
Interindividual and residual variability			
ω_{CL} (%)	29.9	7	
ω_{V1} (%)	18	9	
ω_{V2} (%)	34.7	9	
$\omega_{k\text{out}}$ (%)	46.3	8	
$\omega_{k\text{deg}}$ (%)	90.5	10	
σ_{add} (nmol/L)	8.33	12	
σ_{prop} (%)	20.7	2	

BSA body surface area, $CD20_{cir}$ baseline CD20 count on circulating B cells, *CL* rituximab endogenous clearance, k_{deg} rituximab target-mediated elimination rate constant, k_{in} zero-order production rate constant of target antigen, k_{out} first-order rate constant of rituximab-independent death of latent target antigen, *MTT* mean transit time, Q distribution clearance, *R-FC* fludarabine-cyclophosphamide-rituximab, *RSE* relative standard error [RSE = (estimate/standard error) × 100], V_1 central distribution volume, V_2 peripheral distribution volume, σ_{add} standard deviation of additive residual error, σ_{prop} standard deviation of proportional residual error, ω inter-individual standard deviation

Higher rituximab concentrations were predicted in active Binet stages A and B in comparison to Binet C (Fig. 4e), mainly during the first four cycles. Higher rituximab concentrations and earlier decreases in latent target antigen (L) were predicted in the dense R-FC arm compared with the standard arm in the early treatment cycles, with no major difference in later cycles (Fig. 5). In both treatment arms, no minimum value for L was reached during rituximab treatment, whereas blood lymphocyte counts reached a minimum value approximately 20–50 days after the first rituximab dose (Fig. 6).

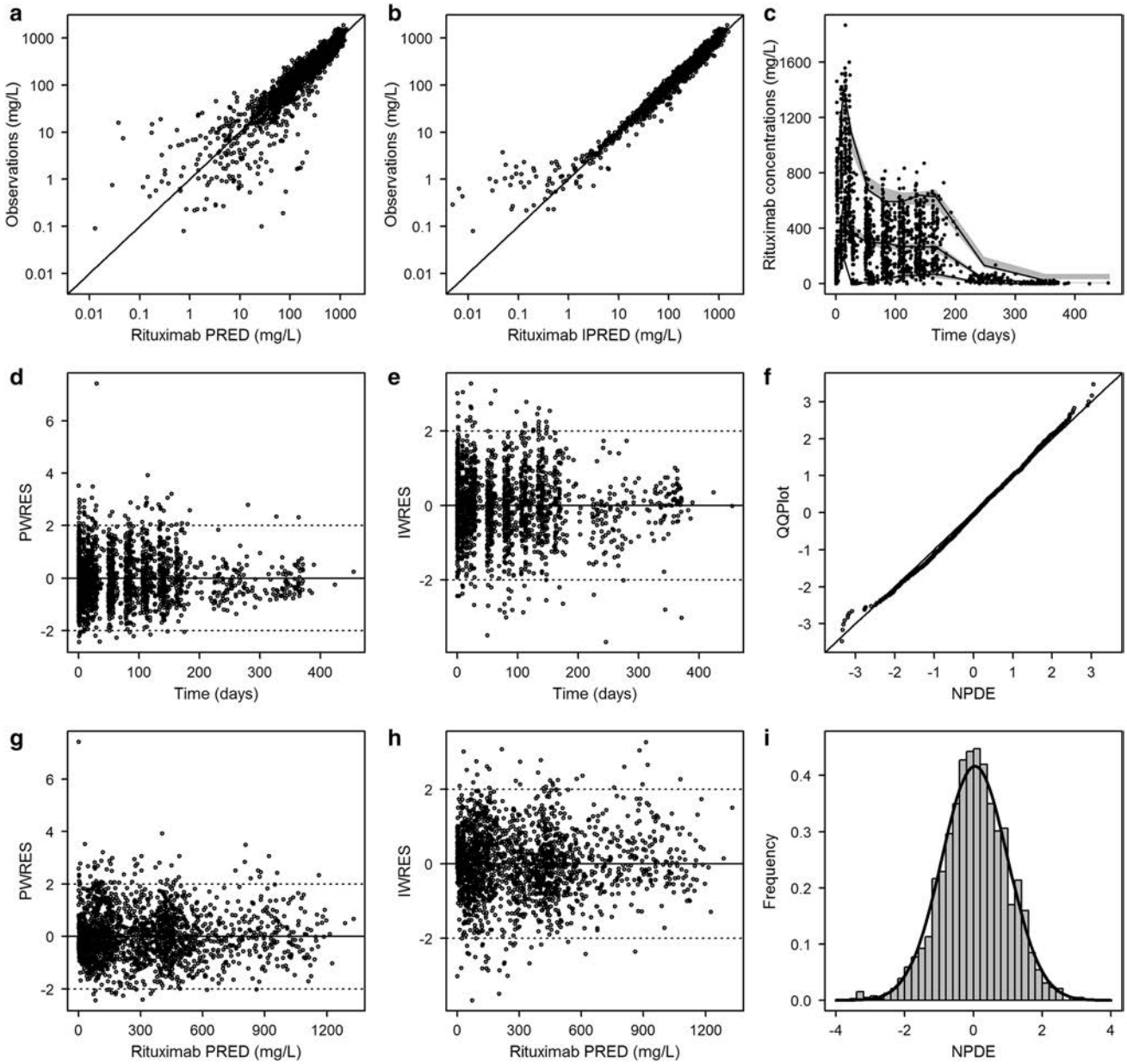

Fig. 2 Goodness-of-fit plots of the final pharmacokinetic model. **a** Rituximab observed vs. population-predicted concentrations (PRED). **b** Observed vs. individual predicted concentrations (IPRED). **c** Visual predictive checks for rituximab concentrations; *circles* are observed concentrations, *solid lines* are 5th, 50th, and 95th percentiles of simulated data, and *shaded areas* are 90% prediction intervals. **d** Population-weighted residuals (PWRES) vs. time. **e** Individual weighted residuals (IWRES) vs. time. **f** Q-Q plot of normalized prediction distribution errors (NPDE). **g** PWRES vs. PRED. **h** IWRES vs. PRED. **i** Distribution frequency of NPDE

4 Discussion

To our knowledge, the present study is the first to describe the influence of baseline target-antigen mass and the *FCGR3A*-158V/F polymorphism on rituximab PK. A semi-mechanistic model including a two-compartment pharmacokinetic model and latent target-antigen turnover accurately described the concentration-time course of rituximab in patients with CLL, and allowed quantifying rituximab elimination by the target-mediated pathway besides the endogenous pathway.

Rituximab PK in CLL was previously described by Li et al. using a two-compartment model with linear and time-dependent clearances [5]. This suggested a potential influence of antigenic burden on clearance, which could not yet be investigated owing to the limited number of patients ($n = 21$). This model was subsequently used to describe the PK of another anti-CD20 antibody, obinutuzumab, in

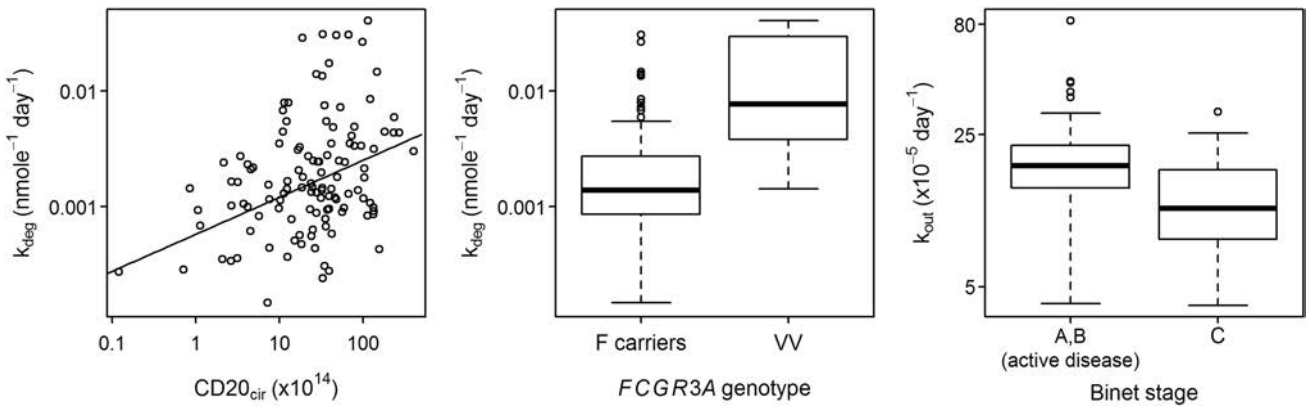

Fig. 3 Predicted model parameters vs. covariates. *Left* rituximab target-mediated elimination rate constant (k_{deg}) vs. baseline CD20 count on circulating B cells ($CD20_{cir}$). *Middle* k_{deg} according to the *FCGR3A*-158V/F polymorphism; the *boxes* represent the 25th, 50th, and 75th percentiles, and the *whiskers* represent the 5th and 95th percentiles. *Right* first-order rate constant of rituximab-independent death of latent target antigen (k_{out}) according to Binet stage

various B-cell malignancies, where disease histology was shown to influence time-dependent clearance [32]. Therefore, to date, there has been no evidence of a direct influence of antigenic mass on rituximab PK in CLL patients. In the present study, our model allowed the description of both rituximab and target-antigen kinetics over time and provided a better description of rituximab concentrations than models including Michaelis–Menten elimination or time-varying clearance. Our model was derived from a previously published model by Friberg et al. describing myelosuppression induced by several chemotherapeutic drugs [29], in which progenitor cell proliferation is modulated by mature cell count. Parameters describing this modulation were not identifiable using our data, probably because of the absence of repeated measurements of the target antigen amount.

The target antigen was included as a latent variable (L, not measured), which is computed using deviation of rituximab PK from linearity. This variable should be interpreted as the amount of CD20 on mature B cells available for rituximab binding. Therefore, L captures CD20 wherever rituximab interacts with it, i.e., including blood and extra-blood compartments (including lymph nodes) and thus provides supplemental information about antigenic target compared with blood lymphocyte count. However, these compartments cannot be distinguished using L.

Measurements of total lymphocyte counts before each rituximab infusion were available in our study. Because CLL total lymphocytes consist predominantly of B cells, one could consider them as a relevant biomarker to model the antigen turnover in the transit compartments. However, because (1) B cells are massively lysed after rituximab administration and do not remain the major type of lymphocytes [33], (2) the time to achieve depletion of CD20 latent target is longer than that for blood lymphocytes, and (3) B-cell depletion occurs both in blood and extra-blood loci (e.g., in lymph nodes), using blood total lymphocyte count as a biomarker in the transit model may introduce a significant bias to the model, probably greater than that of latent variables. Moreover, because no minimum value of L was reached during rituximab treatment in both arms (Figs. 5, 6), there may still remain malignant B cells in some patients, who may therefore benefit from longer rituximab treatment, or a maintenance treatment. This is in accordance with a longer progression-free survival in patients treated with a 2-year maintenance of rituximab compared with those with no rituximab maintenance [34].

Central and peripheral volumes of distribution estimated in the present study were in reasonable agreement with those of the Li et al. study. Linear clearance was similar to that of the Li et al. study (0.14 vs. 0.17 L/day [5], respectively), but not target-mediated (6.4 vs. 1.3 L/day [5] at $t = 0$, respectively) or inter-compartment clearances (0.31 vs. 1.15 L/day [5], respectively). The values of inter-compartment clearances between both modeling strategies may compensate for the differences of target-mediated clearance description.

Rituximab target-mediated elimination rate constant (k_{deg}) increased significantly with the baseline count of CD20 target antigen on circulating B cells ($\mathrm{CD20_{cir}}$). This is consistent with TMDD, a mechanism frequently reported for monoclonal antibodies [9–12]: after the binding of rituximab to the CD20 target antigen, antibody-target antigen complexes are formed, which results in their elimination. This target-mediated clearance is thought to depend not only on antibody concentrations, but also on the target antigen amount, distribution, and turnover. Increased levels of the target antigen result in increased 'consumption' (target-mediated elimination) of the therapeutic

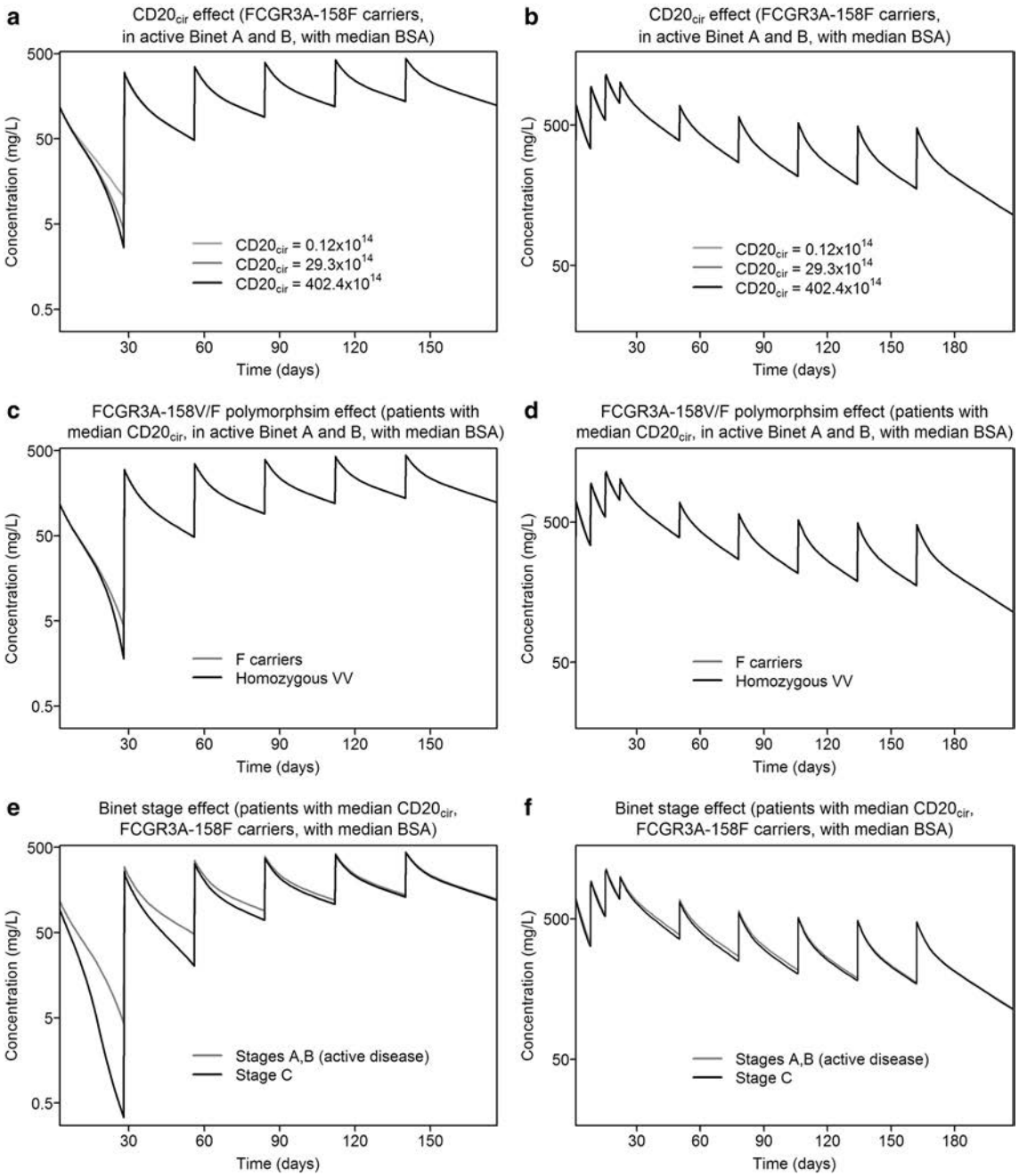

Fig. 4 Model-based simulations of rituximab concentration-time profiles in standard (*left*) and dense (*right*) R-FC arms according to (**a**, **b**) $CD20_{cir}$, (**c**, **d**) *FCGR3A*-158V/F polymorphism, and (**e**, **f**) Binet stage. *BSA* body surface area, $CD20_{cir}$ baseline CD20 count on circulating B cells, *R-FC* fludarabine-cyclophosphamide-rituximab

antibody, leading to an increase in its target-mediated elimination. Our model was a simplified TMDD model because the dissociation of the antibody-antigen complex was not identifiable as target-antigen data were not available over time.

In contrast to $CD20_{cir}$, the baseline CD20 count in the lymph nodes ($CD20_{LN}$) did not significantly influence k_{deg}; as suggested by previous animal studies, rituximab-induced B-cell depletion is delayed and more difficult to achieve in lymph nodes than in peripheral blood [13, 35, 36]. These differences in target-antigen lysis could thus explain the lack of association between $CD20_{LN}$ count on baseline and target-mediated elimination rate. Additionally, a previous study reported lower intensity of surface CD20 expression in the lymph nodes of B-CLL patients than in peripheral blood [37], raising the hypothesis of potential less cytotoxicity triggered by rituximab on lymph node cells, and therefore less important target-mediated elimination.

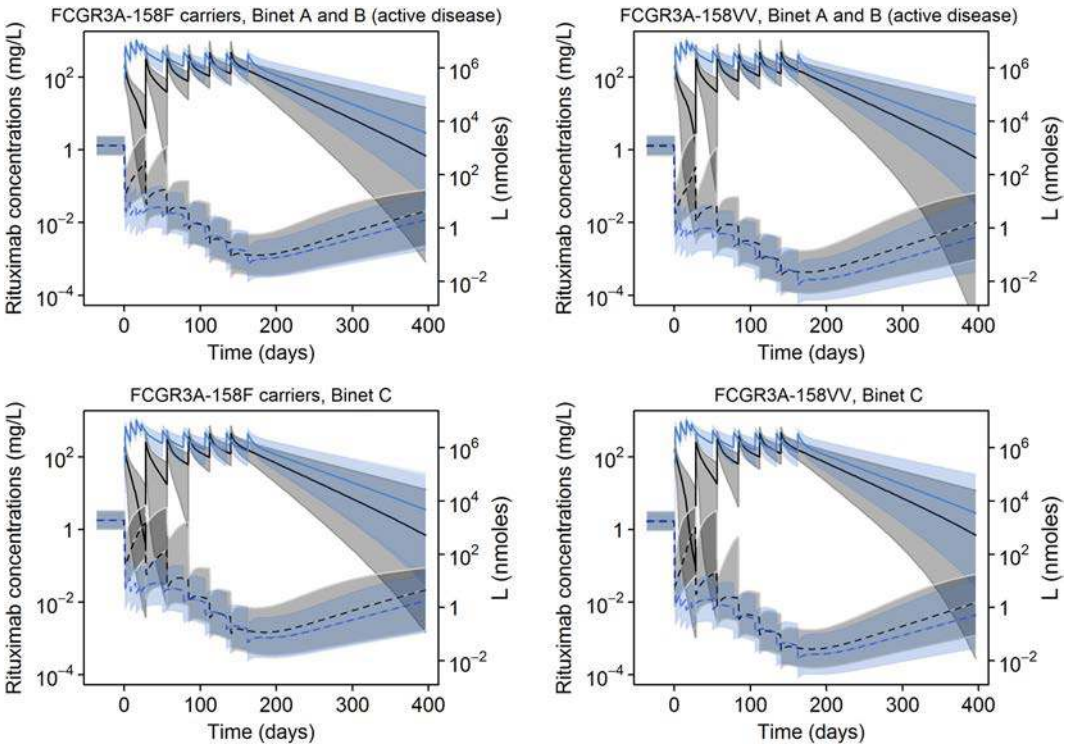

Fig. 5 Model-based simulations of rituximab concentrations (*upper* part of each graph) and latent amount of CD20 expressed on mature B cells available for rituximab binding (*L*, *bottom* part of each graph) in standard (*gray*) and dense (*blue*) R-FC arms in different groups of *FCGR3A*-158V/F genotype and Binet stage. *Shaded areas* represent the 90% confidence intervals, and *lines* represent the 50th percentiles. *R-FC* fludarabine-cyclophosphamide-rituximab

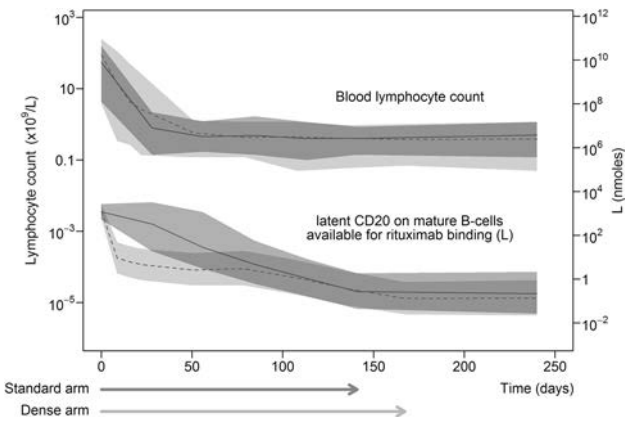

Fig. 6 Profiles of blood lymphocyte count (*upper*) and of the latent amount of CD20 on mature B cells available for rituximab binding (*L*, *bottom*) in standard (*dark gray*) and dense (*light gray*) R-FC arms for active Binet stages A/B and 158F carriers. *Shaded areas* represent the 90% confidence intervals, and *lines* represent the 50th percentiles in standard (*full line*) and dense (*broken line*) arms. *Arrows* represent the duration of treatment for both arms. *R-FC* fludarabine-cyclophosphamide-rituximab

However, CD20 intensity per cell did not influence k_{deg} in our study (data not shown; $p = 0.1$), nor did it influence ADCC in vitro [38] or differ between responders and non-responders in another study in CLL/small lymphocytic leukemia [39, 40], and thus seems not to have a significant impact on rituximab cytotoxicity.

Specific target-mediated elimination was also influenced by the *FCGR3A*-158V/F polymorphism, with higher k_{deg} in *FCGR3A*-158VV patients than in F carriers. Human IgG1 shows a higher affinity for FcγRIIIa-158V compared with FcγRIIIa-158F, resulting in higher natural killer cell recruitment in VV patients than in F carriers [14]. This may explain higher rituximab potency in inducing ADCC with natural killer cells from VV donors compared with FF donors, as well as better response rates in VV patients in rituximab-treated B-cell malignancies [15–17] and malignancies treated with other antibodies acting partly by ADCC [41, 42]. Higher rituximab ADCC potency in VV patients may lead to an increase in rituximab elimination, as was suggested for infliximab, an anti-tumor necrosis factor-α antibody. In Crohn's disease patients, the infliximab elimination rate was higher in VV patients than in F carriers [20]. Our semi-mechanistic model reflecting TMDD supports increased rituximab target-mediated 'consumption' in VV patients compared with F carriers.

Patients in Binet stage C had significantly lower rituximab-independent target death (k_{out}) in comparison to earlier stages A and B. Consistent with our results, peripheral blood lymphocytes from Binet C patients

showed lower spontaneous apoptosis in vitro [43]. Because defective apoptosis is a characteristic feature in CLL pathogenesis [44], patients in the advanced disease stage (Binet C) are expected to exhibit less apoptosis, which may explain the lower rituximab-independent target death compared with earlier disease stages (Binet A/B).

Reasons for higher rituximab endogenous clearance (CL) and V_2 in the dense R-FC arm compared with the standard R-FC arm remain unclear. Following the intensified rituximab pre-phase in the dense arm, the neonatal Fc receptor of IgG (FcRn), which protects IgG from degradation after endocytosis, might be saturated, resulting in higher rituximab CL [45]. This is however subject to caution because FcRn saturation is usually not thought to be achieved with therapeutic concentrations of monoclonal antibodies [46].

Finally, central and peripheral volumes of distribution of rituximab increased with BSA, which is in agreement with previous results obtained with rituximab and other monoclonal antibodies, where body size (weight, BSA) was associated with an increase in volumes of distribution and/or clearance [47–50].

The influence of final model covariates on rituximab concentrations was investigated using model-based simulations. In the standard R-FC arm, increased k_{deg} in patients with higher $CD20_{cir}$ values was associated with lower rituximab concentrations during the first treatment cycle. These differences were not marked after the second administration. This is in agreement with TMDD mechanism, which is most pronounced when the amount of the therapeutic antibody is low relative to the amount of the target antigen [51], leading to a significant contribution of target-mediated elimination to the total clearance of the antibody. After the second injection, owing to increasing rituximab concentrations and a decreasing target antigen amount, the (second-order saturable) target-mediated elimination pathway becomes minimal and thus contributes less to the PK of the antibody, explaining the low influence of $CD20_{cir}$ on rituximab concentrations. In the same way, *FCGR3A*-158VV patients had lower rituximab concentrations than F carriers after the first administration, and nearly similar concentrations in later cycles. Because rituximab concentrations are known to be associated with clinical response [4–7], our findings may explain, at least in part, the similar outcomes of the different *FCGR3A*-158V/F genotype groups previously reported in patients with CLL [18, 19].

In contrast to the standard arm, no differences in rituximab concentrations were observed according to $CD20_{cir}$ or *FCGR3A*-158V/F genotypes in the dense R-FC arm. This can be explained by low amounts of target antigen relative to rituximab from the intensified pre-phase, and therefore a faster saturation of the target-mediated elimination pathway. The contribution of the latter to rituximab PK is thus already minor in the pre-phase, resulting in the lack of influence of $CD20_{cir}$ on rituximab concentrations over the entire treatment period.

5 Conclusion

We developed a semi-mechanistic model including a target-mediated elimination component that accurately described rituximab PK in patients with CLL. This allowed us to show for the first time an influence of a baseline count of target antigen and the *FCGR3A*-158V/F polymorphism on rituximab target-mediated elimination.

Acknowledgements Measurements of rituximab serum concentrations were carried out within the CePiBAc platform. CePiBAc is co-financed by the European Union. Europe is committed to the region center with the European Regional Development Fund. This work was supported by the French Higher Education and Research Ministry under the program 'Investissements d'avenir' Grant Agreement: LabEx MAbImprove ANR-10-LABX-53-01. The authors thank Anne-Claire Duveau, Caroline Guerineau-Brochon, and Céline Desvignes for technical assistance. The authors also thank the reviewers for valuable advice, which led to considerable improvement of the manuscript.

Author's contributions Mira Tout analyzed and interpreted the data, and wrote the manuscript. Anne-Laure Gagez participated in data interpretation and reviewed the manuscript. Stéphane Leprêtre designed the clinical study, was the principal investigator of the clinical study, and reviewed the manuscript. Valérie Gouilleux-Gruart performed genotyping and reviewed the manuscript. Nicolas Azzopardi participated in data analysis and reviewed the manuscript. Alain Delmer acquired data and reviewed the manuscript. Mélanie Mercier acquired data and reviewed the manuscript. Loic Ysebaert acquired data and reviewed the manuscript. Kamel Laribi acquired data and reviewed the manuscript. Hugo Gonzalez acquired data and reviewed the manuscript. Gilles Paintaud designed the study and reviewed the manuscript. Guillaume Cartron designed the clinical study, was the principal investigator of the clinical study, and reviewed the manuscript. David Ternant designed the study, supervised and participated in the writing of the manuscript, and reviewed the manuscript.

Compliance with Ethical Standards

Funding This study was funded by FILO Group and Roche SAS (Neuilly, France).

Conflict of interest Mira Tout, Anne-Laure Gagez, Stéphane Leprêtre, Valérie Gouilleux-Gruart, Nicolas Azzopardi, Alain Delmer, Mélanie Mercier, Loic Ysebaert, Kamel Laribi, and Hugo Gonzalez have no conflicts of interest to declare. Gilles Paintaud reports grants received by his research team from Novartis, Roche Pharma, Genzyme, MSD, Chugai, and Pfizer. Guillaume Cartron received consultancy fees from Roche and Celgene, honorarium from Roche, Celgene, Jansen, Gilead, and Sanofi, and travel arrangement from Jansen, Gilead, and Sanofi. David Ternant has given lectures for Sanofi and Amgen.

References

1. Hallek M, Fischer K, Fingerle-Rowson G, et al. Addition of rituximab to fludarabine and cyclophosphamide in patients with chronic lymphocytic leukaemia: a randomised, open-label, phase 3 trial. Lancet. 2010;376:1164–74.
2. Tam CS, O'Brien S, Wierda W, et al. Long-term results of the fludarabine, cyclophosphamide, and rituximab regimen as initial therapy of chronic lymphocytic leukemia. Blood. 2008;112:975–80.
3. Robak T, Dmoszynska A, Solal-Céligny P, et al. Rituximab plus fludarabine and cyclophosphamide prolongs progression-free survival compared with fludarabine and cyclophosphamide alone in previously treated chronic lymphocytic leukemia. J Clin Oncol. 2010;28:1756–65.
4. Berinstein NL, Grillo-López A, White CA, et al. Association of serum eituximab (IDEC-C2B8) concentration and anti-tumor response in the treatment of recurrent low-grade or follicular non-Hodgkin's lymphoma. Ann Oncol. 1998;9:995–1001.
5. Li J, Zhi J, Wenger M, Valente N, et al. Population pharmacokinetics of rituximab in patients with chronic lymphocytic leukemia. J Clin Pharmacol. 2012;52:1918–26.
6. Igarashi T, Kobayashi Y, Ogura M, et al. Factors affecting toxicity, response and progression-free survival in relapsed patients with indolent B-cell lymphoma and mantle cell lymphoma treated with rituximab: a Japanese phase II study. Ann Oncol. 2002;13:928–43.
7. Tobinai K, Igarashi T, Itoh K, et al. Japanese multicenter phase II and pharmacokinetic study of rituximab in relapsed or refractory patients with aggressive B-cell lymphoma. Ann Oncol. 2004;15:821–30.
8. Daydé D, Ternant D, Ohresser M, et al. Tumor burden influences exposure and response to rituximab: pharmacokinetic-pharmacodynamic modeling using a syngeneic bioluminescent murine model expressing human CD20. Blood. 2009;113:3765–72.
9. Panoilia E, Schindler E, Samantas E, et al. A pharmacokinetic binding model for bevacizumab and VEGF165 in colorectal cancer patients. Cancer Chemother Pharmacol. 2015;75:791–803.
10. Gibiansky L, Sutjandra L, Doshi S, et al. Population pharmacokinetic analysis of denosumab in patients with bone metastases from solid tumours. Clin Pharmacokinet. 2012;51:247–60.
11. Gibiansky L, Gibiansky E. Target-mediated drug disposition model: relationships with indirect response models and application to population PK-PD analysis. J Pharmacokinet Pharmacodyn. 2009;36:341–51.
12. Dirks N, Meibohm B. Population pharmacokinetics of therapeutic monoclonal antibodies. Clin Pharmacokinet. 2010;49:633–59.
13. Reff M, Carner K, Chambers K, et al. Depletion of B cells in vivo by a chimeric mouse human monoclonal antibody to CD20. Blood. 1994;83:435–45.
14. Koene HR, Kleijer M, Algra J, et al. FcγRIIIa-158V/F polymorphism influences the binding of IgG by natural killer cell Fc γRIIIa, independently of the FcγRIIIa-48L/R/H phenotype. Blood. 1997;90:1109–14.
15. Cartron G, Dacheux L, Salles G, et al. Therapeutic activity of humanized anti-CD20 monoclonal antibody and polymorphism in IgG Fc receptor FcγrIIIa gene. Blood. 2002;99:754–8.
16. Weng W-K, Levy R. Two immunoglobulin G fragment C receptor polymorphisms independently predict response to rituximab in patients with follicular lymphoma. J Clin Oncol. 2003;21:3940–7.
17. Kim DH, Du Jung H, Kim JG, et al. FCGR3A gene polymorphisms may correlate with response to frontline R-CHOP therapy for diffuse large B-cell lymphoma. Blood. 2006;108:2720–5.
18. Farag SS, Flinn IW, Modali R, et al. Fc gamma RIIIa and Fc gamma RIIa polymorphisms do not predict response to rituximab in B-cell chronic lymphocytic leukemia. Blood. 2004;103:1472–4.
19. Dornan D, Spleiss O, Yeh R-F, et al. Effect of FCGR2A and FCGR3A variants on CLL outcome. Blood. 2010;116:4212–22.
20. Ternant D, Berkane Z, Picon L, et al. Assessment of the influence of inflammation and FCGR3A genotype on infliximab pharmacokinetics and time to relapse in patients with Crohn's eisease. Clin Pharmacokinet. 2015;54:551–62.
21. Hallek M, Cheson BD, Catovsky D, et al. Guidelines for the diagnosis and treatment of chronic lymphocytic leukemia: a report from the International Workshop on Chronic Lymphocytic Leukemia updating the National Cancer Institute-Working Group 1996 guidelines. Blood. 2008;111:5446–56.
22. Binet JL, Auquier A, Dighiero G, et al. A new prognostic classification of chronic lymphocytic leukemia derived from a multivariate survival analysis. Cancer. 1981;48:198–206.
23. Blasco H, Lalmanach G, Godat E, et al. Evaluation of a peptide ELISA for the detection of rituximab in serum. J Immunol Methods. 2007;325:127–39.
24. Dall'Ozzo S, Andres C, Bardos P, et al. Rapid single-step FCGR3A genotyping based on SYBR Green I fluorescence in real-time multiplex allele-specific PCR. J Immunol Methods. 2003;277:185–92.
25. Campo E, Swerdlow SH, Harris NL, et al. The 2008 WHO classification of lymphoid neoplasms and beyond: evolving concepts and practical applications. Blood. 2011;117:5019–32.
26. Nougaret S, Jung B, Aufort S, et al. Adrenal gland volume measurement in septic shock and control patients: a pilot study. Eur Radiol. 2010;20:2348–57.
27. Pearson TC, Guthrie DL, Simpson J, et al. Interpretation of measured red cell mass and plasma volume in adults: Expert Panel on Radionuclides of the International Council for Standardization in Haematology. Br J Haematol. 1995;89:748–56.
28. Alexander HD, Markey GM, Nolan RL, Morris TC. Cell sizing in chronic lymphoproliferative disorders: an aid to differential diagnosis. J Clin Pathol. 1992;45:875–9.
29. Friberg LE, Henningsson A, Maas H, et al. Model of chemotherapy-induced myelosuppression with parameter consistency across drugs. J Clin Oncol. 2002;20:4713–21.
30. van Kesteren C, Zandvliet AS, Karlsson MO, et al. Semi-physiological model describing the hematological toxicity of the anticancer agent indisulam. Invest New Drugs. 2005;23:225–34.
31. Comets E, Brendel K, Mentré F. Computing normalised prediction distribution errors to evaluate nonlinear mixed-effect models: the npde add-on package for R. Comput Methods Programs Biomed. 2008;90:154–66.
32. Gibiansky E, Gibiansky L, Carlile DJ, et al. Population pharmacokinetics of obinutuzumab (GA101) in chronic lymphocytic leukemia (CLL) and non-Hodgkin's lymphoma and exposure-response in CLL. CPT Pharmacomet Syst Pharmacol. 2014;3:e144.
33. Huhn D, von Schilling C, Wilhelm M, et al. Rituximab therapy of patients with B-cell chronic lymphocytic leukemia. Blood. 2001;98:1326–31.
34. Greil R, Obrtlíková P, Smolej L, et al. Rituximab maintenance versus observation alone in patients with chronic lymphocytic leukaemia who respond to first-line or second-line rituximab-containing chemoimmunotherapy: final results of the AGMT CLL-8a Mabtenance randomised trial. Lancet Haematol. 2016;3:e317–29.
35. Gong Q, Ou Q, Ye S, et al. Importance of cellular microenvironment and circulatory dynamics in B cell immunotherapy. J Immunol. 2005;174:817–26.

36. Schröder C, Azimzadeh AM, Wu G, et al. Anti-CD20 treatment depletes B-cells in blood and lymphatic tissue of cynomolgus monkeys. Transpl Immunol. 2003;12:19–28.
37. Huh YO, Keating MJ, Saffer HL, et al. Higher levels of surface CD20 expression on circulating lymphocytes compared with bone marrow and lymph nodes in B-cell chronic lymphocytic leukemia. Am J Clin Pathol. 2001;116:437–43.
38. van Meerten T, van Rijn RS, Hol S, et al. Complement-induced cell death by rituximab depends on CD20 expression level and acts complementary to antibody-dependent cellular cytotoxicity. Clin Cancer Res. 2006;12:4027–35.
39. Tam CS, Otero-Palacios J, Abruzzo LV, et al. Chronic lymphocytic leukaemia CD20 expression is dependent on the genetic subtype: a study of quantitative flow cytometry and fluorescent in-situ hybridization in 510 patients. Br J Haematol. 2008;141:36–40.
40. Perz J, Topaly J, Fruehauf S, et al. Level of CD 20-expression and efficacy of rituximab treatment in patients with resistant or relapsing B-cell prolymphocytic leukemia and B-cell chronic lymphocytic leukemia. Leuk Lymphoma. 2002;43:149–51.
41. Zhang W, Gordon M, Schultheis AM, et al. FCGR2A and FCGR3A polymorphisms associated with clinical outcome of epidermal growth factor receptor expressing metastatic colorectal cancer patients treated with single-agent cetuximab. J Clin Oncol. 2007;25:3712–8.
42. Musolino A, Naldi N, Bortesi B, et al. Immunoglobulin G fragment C receptor polymorphisms and clinical efficacy of trastuzumab-based therapy in patients with HER-2/neu-positive metastatic breast cancer. J Clin Oncol. 2008;26:1789–96.
43. Oliveira GB, Pereira FG, Metze K, Lorand-Metze I. Spontaneous apoptosis in chronic lymphocytic leukemia and its relationship to clinical and cell kinetic parameters. Cytometry. 2001;46:329–35.
44. Billard C. Apoptosis inducers in chronic lymphocytic leukemia. Oncotarget. 2014;5:309–25.
45. Junghans RP. IgG biosynthesis: no “immunoregulatory feedback”. Blood. 1997;90:3815–8.
46. Wang W, Wang E, Balthasar J. Monoclonal antibody pharmacokinetics and pharmacodynamics. Clin Pharmacol Ther. 2008;84:548–58.
47. Müller C, Murawski N, Wiesen MHJ, et al. The role of sex and weight on rituximab clearance and serum elimination half-life in elderly patients with DLBCL. Blood. 2012;119:3276–84.
48. Ternant D, Mulleman D, Lauféron F, et al. Influence of methotrexate on infliximab pharmacokinetics and pharmacodynamics in ankylosing spondylitis. Br J Clin Pharmacol. 2011;73:55–65.
49. Azzopardi N, Lecomte T, Ternant D, et al. Cetuximab pharmacokinetics influences progression-free survival of metastatic colorectal cancer patients. Clin Cancer Res. 2011;17:6329–37.
50. Ng CM, Bruno R, Combs D, Davies B. Population pharmacokinetics of rituximab (anti-CD20 monoclonal antibody) in rheumatoid arthritis patients during a phase II clinical trial. J Clin Pharmacol. 2005;45:792–801.
51. Tabrizi MA, Tseng C-ML, Roskos LK. Elimination mechanisms of therapeutic monoclonal antibodies. Drug Discov Today. 2006;11:81–8.